BBA - Molecular Basis of Disease 1870 (2024) 167171

Contents lists available at ScienceDirect

BBA - Molecular Basis of Disease

journal homepage: www.elsevier.com/locate/bbadis

High phosphate and calcium induce osteoblastic phenotype switching and calcification of corneal epithelial cells in a Runx2-dependent and synergistic manner; a possible mechanism of chronic kidney disease-associated corneal calcification

Haneen Ababneh [a,b], Andrea Tóth [a], Gréta Lente [a,b], Enikő Balogh [a], Dávid Máté Csiki [a,b], Béla Nagy Jr [c], Árpád Szöőr [d], Viktória Jeney [a,*]

[a] MTA-DE Lendület Vascular Pathophysiology Research Group, Research Centre for Molecular Medicine, Faculty of Medicine, University of Debrecen, Debrecen, Hungary
[b] Doctoral School of Molecular Cell and Immune Biology, Faculty of Medicine, University of Debrecen, Debrecen, Hungary
[c] Department of Laboratory Medicine, Faculty of Medicine, University of Debrecen, Debrecen, Hungary
[d] Department of Biophysics and Cell Biology, Faculty of Medicine, University of Debrecen, Debrecen, Hungary

ARTICLE INFO

Keywords:
Chronic kidney disease (CKD)
Corneal calcification
Runx2
Corneal epithelial cells
Osteogenic phenotype switch
Ectopic calcification

ABSTRACT

Patients with advanced chronic kidney disease (CKD) have elevated circulating calcium × phosphate product levels and exhibit soft tissue calcification. Besides the cardiovascular system, calcification is commonly observed in the cornea in CKD patients on hemodialysis. Cardiovascular calcification is a cell-mediated, highly regulated process, and we hypothesized that a similar regulatory mechanism is implicated in corneal calcification with the involvement of corneal epithelial cells (CECs). We established a mouse model of CKD-associated corneal calcification by inducing CKD in DBA/2J mice with an adenine and high phosphate diet. CKD was associated with aorta and corneal calcification as detected by OsteoSense staining and corneal Ca measurement (1.67-fold elevation, $p < 0.001$). *In vitro*, excess phosphate and Ca induced human CEC calcification in a dose-dependent and synergistic manner, without any influence on cell viability. High phosphate and Ca-containing osteogenic medium (OM; 2.5 mmol/L excess phosphate and 0.6 mmol/L excess Ca over control) increased the protein expression of Runx2 and induced its nuclear translocation. OM increased the expression of the bone-specific Ca-binding protein osteocalcin (130-fold increase, $p < 0.001$). Silencing of Runx2 attenuated OM-induced CEC calcification. Immunohistology revealed upregulation of Runx2 and overlapping between the Runx2 and the Alizarin red positive areas of calcification in the cornea of CKD mice. This work sheds light on the mechanism of CKD-induced corneal calcification and provides tools to test calcification inhibitors for the prevention of this detrimental process.

1. Introduction

Chronic kidney disease (CKD) is a global public health problem, with an estimated prevalence of 13.4 % [1]. Advanced CKD (stages 4 and 5) is associated with the elevation of the Ca × phosphate product concentration and the deposition of the excess phosphate and Ca in the form of hydroxyapatite in soft tissues [2]. Heterotopic mineralization of the cardiovascular system (aorta, heart valves) is a very frequent complication, and an important contributor to the high cardiovascular risk of CKD patients [2].

Besides the cardiovascular system, corneal and conjunctival calcifications (CCC) are commonly observed in CKD patients on hemodialysis

Abbreviations: AR, Alizarin red; Ca, calcium; CCC, corneal and conjunctival calcifications; CECs, corneal epithelial cells; CKD, chronic kidney disease; Ctrl, control; DAPI, 4′,6-diamidino-2-phenylindole; DMEM, Dublecco's modified eagle medium; DMSO, dimethyl sulphoxide; H&E, hematoxylin and eosin; ECM, extracellular matrix; EDTA, ethylenediamine-tetraacetic acid; ELISA, enzyme-linked immunosorbent assay; FBS, fetal bovine serum; MTT, 3-[4,5-dimethylthiazol-2-yl]-2,5-diphenyl-tetrazolium bromide; OCN, osteocalcin; OD, optical density; OM, osteogenic medium; PBS, phosphate-buffered saline; PFA, paraformaldehyde; Pi, inorganic phosphate; Runx2, runt-related transcription factor 2; VICs, valve interstitial cells; VSMCs, vascular smooth muscle cells.

* Corresponding author.
E-mail address: jeney.viktoria@med.unideb.hu (V. Jeney).

https://doi.org/10.1016/j.bbadis.2024.167171
Received 10 January 2024; Received in revised form 4 April 2024; Accepted 10 April 2024
Available online 16 April 2024

treatment [3,4]. In previous studies, the prevalence of CCC was found to be as high as 82.7–87.3 % among CKD patients who were on dialysis therapy for >6 months [5,6]. The symptoms of CCC include decreased or blurred vision, foreign body sensation in the eye, irritation, redness, and light intolerance. CCC treatment options mostly target the symptoms and not the cause of the disease. Among them, surgical mechanical debridement and ethylene-diamine-tetra-acetic acid (EDTA) chelation therapy are the most common techniques [7].

Some studies found an association between CCC and vascular calcification and revealed that the severity of CCC is an independent predictor for all-cause one-year mortality in CKD patients under hemodialysis [5,8]. However, others found no correlation between CCC and coronary calcium scores [6].

Vascular calcification in CKD is an active process in which phenotypic switching of vascular smooth muscle cells (VSMC) into osteoblast-like cells occurs [9]. Runx2, a key transcription factor that regulates osteoblast and chondrocyte differentiation, has been shown to orchestrate high phosphate-induced lineage reprogramming of VSMC towards osteo-/chondrogenesis [10]. This notion is supported by the finding that VSMC-specific Runx2-deficiency is associated with the inhibition of high-fat diet-induced calcification in mice [11].

We lack knowledge of whether hydroxyapatite deposition in the cornea – similar to vascular calcification – is the result of an active process, or CCC is a passive/degenerative process. Corneal epithelial cells (CECs) express Runx2 [12], and genome-wide association studies identified Runx2 as one of the top genes related to central corneal thickness [13,14], and corneal biomechanics [15]. However, we lack information on whether CECs can undergo osteo-/chondrogenic differentiation and whether Runx2 plays a role in it. In this work, we aimed to establish an *in vivo* model of CKD-induced corneal calcification and to investigate the capability and regulation of osteo-/chondrogenic differentiation of CECs.

2. Materials and methods

2.1. Induction of CKD in mice

All the mice were housed in a temperature- (22 °C) and light-controlled (12-h light/12-h dark) room, in cages with standard beddings and unlimited access to food and water. Female DBA/2 J mice (8–12 weeks old, n = 24) were randomly divided into 2 groups, control (Ctrl) and CKD. CKD was induced by a two-phase diet as described previously [16]. In the first 6 weeks, the CKD mice received a diet containing 0.2 % adenine and 0.7 % phosphate, followed by a diet supplemented with 0.2 % adenine and 1.8 % phosphate (S8106-S075 and S8893-S006 respectively; Ssniff) for 6 weeks. Control mice received a standard rodent diet containing 0.3 % phosphate throughout the experiment. At the end of the experiments, mice were euthanized by CO_2 inhalation, blood was collected by cardiac puncture into citrate-containing tubes, and the aortas and eyes were harvested for analysis. Animal care and experimental procedures were performed following the institutional and national guidelines and were approved by the Institutional Ethics Committee of the University of Debrecen under registration number 10/2021/DEMÁB. Animal studies were reported in compliance with the ARRIVE guidelines.

2.2. Laboratory analysis of renal function in mice

Plasma phosphate, calcium urea, and creatinine levels were evaluated by kinetic assays on a Cobas® c502 device (Roche Diagnostics).

2.3. Imaging and quantification of aortic and eye calcification

OsteoSense dye (OsteoSense 750 EX, NEV10020EX, PerkinElmer) and near-infrared imaging were used to evaluate aorta calcification in mice as previously described [17]. One day before the end of the experiment, mice were anesthetized with isoflurane inhalation and injected with OsteoSense dye in a dose of 2 nmol/20 g body weight through the retro-orbital venous sinus. Imaging was performed 24 h post-injection. The mice were euthanized with CO_2 inhalation, then perfused with 5 mL of ice-cold PBS, and the isolated aortas and eyes were analyzed *ex-vivo* with IVIS Spectrum *In Vivo* Imaging System (PerkinElmer).

2.4. Histology

Eight eyes (4 in each group) were fixed in 10 % neutral-buffered formalin and embedded in paraffin blocks. Subsequently, they were cut into 4 μm-thick cross-sections. The sections were deparaffinized and rehydrated, followed by von Kossa and Alizarin red using standard procedures. For von Kossa staining, the sections were placed in fresh 1 % silver nitrate under UV light for 1 h, washed with fresh 5 % sodium thiosulfate for 5 min, and counterstained with nuclear fast for 5 min. For Alizarin red S staining, sections were stained for 5 min in 2 % alizarin red S (pH 4.2). All sections were dehydrated using a graded alcohol series and mounted. All the sections were counterstained with Hematoxylin and Eosin.

2.5. Immunohistochemistry staining

Paraffin-embedded eye sections (4 μm thick) were deparaffinized with xylene and then rehydrated with a graded series of ethanol. Afterward, heat-mediated antigen retrieval was performed in the universal HIER antigen retrieval reagent (ab208572, Abcam), and the slides were then incubated with an anti-Runx2 antibody (Sc-390715, Santa Cruz, 1:100), at 4 °C overnight. Endogenous peroxidase activity was blocked with a peroxidase-blocking solution (30 % H_2O_2 in methanol) for 30 min, slides were then incubated with anti-mouse IgG H&L (HRP polymer, ab214879, Abcam) for 1 h and stained with DAB substrate (ab64238, Abcam). The nuclei were counter-stained by a Hematoxylin and Eosin solution.

2.6. Cell culture and treatments

Human corneal epithelial cells (CECs) (P10871, Innoprot) were maintained in DMEM (D6171, Sigma) medium supplemented with 10 % FBS (10270-106, Gibco), antibiotic antimycotic solution (A5955, Sigma) sodium pyruvate (S8636, Sigma) and L-glutamine (G7513, Sigma). Cells were cultured at 37 °C in a humidified atmosphere containing 5 % CO_2. All experiments were performed on confluent CECs between passages 4 and 10. To induce calcification, we exposed CECs to an osteogenic medium that was prepared by supplementing growth medium with different concentrations of inorganic phosphate (NaH_2PO_4-Na_2HPO_4, 1.5–3.0 mmol/L, pH 7.4) and calcium ($CaCl_2$, 0.3 or 0.6 mmol/L). Both growth medium and osteogenic medium were replaced every other day.

2.7. Alizarin Red (AR) staining and quantification

After washing with DPBS, the cells were fixed in 4 % paraformaldehyde (PFA; 16005, Sigma) and rinsed with deionized water thoroughly. Cells were stained with Alizarin Red S (A5533, Sigma) solution (2 %, pH 4.2) for 20 min at room temperature. Excessive dye was removed by several washes in deionized water. To quantify AR staining in 96-well plates, we added 100 μL of hexadecylpyridinium chloride (C9002, Sigma) solution (100 mmol/L) to the wells and measured optical density (OD) at 560 nm, using hexadecylpyridinium chloride solution as blank.

2.8. Quantification of Ca deposition

Cells were washed with DPBS and decalcified with HCl (0.6 mol/L) for 30 min. The Ca content of the HCl supernatant was determined using

the QuantiChrome Calcium Assay Kit (DICA-500, Gentaur). After decalcification, cells were washed with DPBS and lysed with NaOH (0.1 mol/L) and sodium dodecyl sulfate (0.1 %) lysis buffer to collect protein content, which was measured with the BCA protein assay kit (Thermo-Fisher). The Ca content of the cells was normalized to the protein content and expressed as mg/mg protein.

2.9. Determination of cell viability

To determine cell viability MTT assay was performed. Following cell treatment, the cells were washed with PBS, then 3-[4,5-Dimethylthiazol-2-yl]-2,5-diphenyl-tetrazolium bromide solution (MTT, ML2128, Sigma, 0.5 mg/mL) was added. After 4 h of incubation at 37 °C, the MTT solution was removed, and then formazan crystals were dissolved in DMSO. Optical density was measured at 570 nm.

2.10. Western blot

To evaluate protein expression cells were lysed with 2× Laemmli buffer (Sigma). Whole-cell lysates were then resolved in SDS-PAGE (1 and then blotted onto a nitrocellulose membrane (10600002, Amersham Biosciences). Afterward, membranes were incubated with an anti-Runx2 antibody (20700-1-AP, Proteintech, 1:500) overnight at 4 °C, followed by the HRP-labeled anti-rabbit IgG secondary antibody (NA-934, Amersham Biosciences). Antigen-antibody complexes were detected by enhanced chemiluminescence using Clarity™ Western ECL Substrate (170-5061, Bio-Rad Laboratories). Chemiluminescent signals were detected by an X-ray film or digitally using a C-Digit Blot Scanner (LI-COR Biosciences). After detection, the membranes were reprobed for β-actin using an anti-β-actin antibody at a dilution of 1:4000 (sc-47778, Santa Cruz Biotechnology). Blots were quantified by using the inbuilt software on the C-Digit Blot Scanner (LI-COR Biosciences).

2.11. Immunofluorescence staining

CECs were cultured on glass coverslips placed in 12-well plates. Following the treatment, the cells were washed with cold PBS, fixed with 4 % PFA for 10 min at room temperature, and permeabilized with 0.1 % Triton X-100 solution for 15 min. The coverslips were then blocked with 1 % BSA for 45 min, then they were incubated with anti-Runx2 antibody (sc-390715, Santa Cruz Biotechnology, 1:200) overnight at 4 °C. After that they were incubated with goat anti-mouse IgG-CFL 488 antibody (A28175, Invitrogen, 1:300) for an hour at room temperature. To stain the nucleus CECs were counterstained with DAPI (4′,6-diamidino-2-phenylindole, 62248, Thermo Fisher Scientific) at the dilution of 1:1000.

2.12. RNA silencing

CECs were transfected with siRNA with Lipofectamine RNAiMAX transfection reagent (13778–150, Invitrogen), according to the manufacturer's protocol. The siRNA for Runx2 (AM16708, ID: 115587), and silencer negative control #1 (4390843) were purchased from Invitrogen. To confirm the efficiency of silencing we performed a Western blot analysis.

2.13. Quantification of osteocalcin (OCN)

For OCN detection, the extracellular matrix (ECM) of the cells, which were grown on 6-well plates was dissolved in 100 μL of EDTA (E6758, Sigma, 0.5 mol/L, pH 6.9). OCN content of the EDTA-solubilized ECM samples was quantified by an enzyme-linked immunosorbent assay (ELISA) (DY1419-05, DuoSet ELISA, R&D) according to the manufacturer's protocol.

2.14. Statistical analysis

Data are presented as mean ± SD with individual data points. Statistical analyses were performed with GraphPad Prism software (version 8.01). An unpaired two-tailed *t*-test was used to calculate *p* values when two groups were compared. Comparisons between more than two groups were carried out by one-way ANOVA followed by Tukey's multiple-comparisons test. A value of $p < 0.05$ was considered significant.

3. Results

3.1. CKD is associated with the deposition of hydroxyapatite in the cornea

We induced CKD in female DBA/2 J mice with a diet containing adenine (0.2 %) and elevated phosphate (0.7 %) for 6 weeks, then phosphate content of the diet was further increased up to 1.8 % and mice received this diet for an additional 6 weeks. Control mice (Ctrl) received a normal rodent diet with 0.3 % phosphate content (Fig. 1a). CKD was associated with increased plasma urea, creatinine, and phosphate levels, while calcium levels remained unchanged (Fig. 1b–e). We used OsteoSense, a hydroxyapatite-specific near-infrared fluorescent imaging agent, to investigate aorta and eye calcification. We injected the mice with OsteoSense dye (2 nmol/25 g body weight) intravenously. Organs were collected for analysis 24 h post-injection. As we expected fluorescent intensities of the aortas were higher in CKD mice compared to control mice with normal renal function (Fig. 1f). Interestingly, besides the aorta, we found massive hydroxyapatite deposition in the eyes derived from CKD mice (Fig. 1g–h).

Next, we dissected the eyes into the corneal part, the lens, and the retinal part, and found out that the OsteoSense signal is derived from the cornea (Fig. 2a–b). Corneal Ca content was elevated in CKD mice compared to Ctrl (1.67-fold, $p < 0.001$) (Fig. 2c). To identify the exact location and pattern of calcification we performed Alizarin red and von Kossa stainings of eye sections from CKD and Ctrl mice. The eyes of Ctrl mice showed no staining; however, we detected Alizarin red and von Kossa positive pocket-like structures in between the corneal epithelial and stromal layers in the eyes of CKD mice (Fig. 2d).

3.2. Elevated Pi and Ca synergistically induce calcification of human corneal epithelial cells (CECs)

To investigate whether CECs could actively participate in the CKD-associated corneal calcification, we exposed CECs to osteogenic medium (OM) containing different concentrations of excess phosphate (1.5–3.0 mmol/L) and Ca (0.3; 0.6 mmol/L) for 10 days. Calcification was detected by Alizarin red staining which revealed that elevated phosphate and Ca induced extracellular matrix (ECM) calcification of CECs in a synergistic manner (Fig. 3a–b). This result was confirmed by the measurement of the Ca content of the HCl-solubilized ECM (Fig. 3c). OM treatment did not influence cell viability which was determined with MTT assay (Fig. 3d).

3.3. Runx2 regulates OM-induced osteogenic differentiation and calcification of CECs and is upregulated in the calcified cornea of CKD mice

The transcriptional regulator Runx2 plays an essential role in the osteogenic differentiation of mesenchymal stem cells as well as VSMCs, therefore, next, we investigated their role in CECs calcification. To see whether OM treatment induces the expression of Runx2 we performed a time-course experiment and measured Runx2 expression after 24, 48, and 72 h of exposure (Fig. 4a). We found a slight increase in Runx2 expression at the 48- and 72-h time points (Fig. 4a–b). Then we investigated the cellular localization of Runx2 with immunofluorescent microscopy. In the Ctrl cells, Runx2 was present mostly in the cytoplasm.

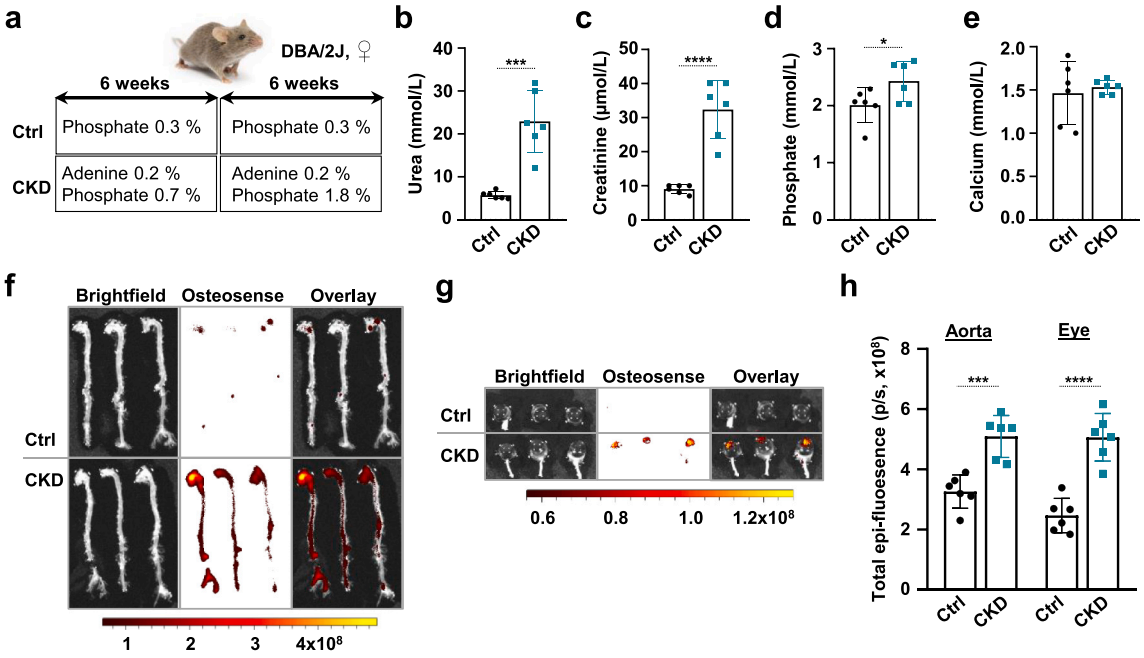

Fig. 1. Calcification in the aorta and eyes of mice with CKD.
(a) CKD was induced with a two-phase diet in female DBA/2J mice. Scheme of the experimental protocol. (b) Plasma urea, (c) plasma creatinine, (d) plasma phosphate (e) plasma calcium levels in control (Ctrl) and CKD mice (n = 6/group), Bright-field and macroscopic fluorescence reflectance imaging and quantification of OsteoSense staining intensity of aortas (f, h) and eyes (g, h) from Ctrl and CKD mice (n = 6/group). Data are expressed as mean ± SD. Ordinary one-way ANOVA followed by Tukey's multiple comparisons test was used to calculate *p* values. $*p < 0.05$, $***p < 0.005$, $****p < 0.001$.

Only about 10 % of the cells showed strong nuclear Runx2 staining (Fig. 4c–d). In contrast, in OM-treated cells, we observed nuclear translocation of Runx2 in nearly all (96 %) of the cells after a 24-h exposure (Fig. 4c–d). Then we measured the expression of osteocalcin (OCN), a bone-specific Ca-binding ECM protein, under the transcriptional regulation of Runx2. We found a 130-fold increase in OCN level in the EDTA-solubilized ECM samples of OM-treated samples compared to Ctrl CECs (Fig. 4e).

To prove the critical involvement of Runx2 in CEC calcification we used a target-specific siRNA to knock down Runx2 expression. With this approach, we could decrease the Runx2 expression that was evaluated by western blot (Fig. 5a–b). Knock-down of Runx2 was associated with decreased OM-induced calcification as determined by alizarin red staining (Fig. 5c–d) and ECM Ca measurement (Fig. 5e). Finally, we wanted to investigate whether Runx2 was involved in corneal calcification in our *in vivo* CKD model. To this end, we performed immunohistology on the eyes of Ctrl and CKD mice and investigated the protein expression of Runx2. We found that Runx2 expression was strongly upregulated in the eyes of CKD mice compared to Ctrl and observed that the Runx2 and the Alizarin red positive areas of calcifications were overlapping in the cornea of CKD mice (Fig. 5f).

4. Discussion

Corneal calcification is a chronic condition, characterized by the deposition of calcium hydroxyapatite salt on the corneal surface. It is a frequent eye complication of dialysis-dependent CKD [3,4]. CKD is accompanied by the elevation of Ca × phosphate product concentration, and its spontaneous precipitation in the oversaturated milieu is considered to be the mechanism of CKD-associated corneal calcification [18].

In this work, we have challenged this consideration and tested the hypothesis that corneal calcification, similarly to vascular calcification, is an active, cell-mediated process. We report for the first time that CEC calcification *in vitro* can be triggered by elevated Ca and phosphate levels. CEC calcification is accompanied by nuclear translocation of the master osteogenic transcription factor Runx2. We observed a notable synergistic effect of Ca and phosphate in combination on CEC calcification, corroborating earlier reports showing that elevated Ca and phosphate induce calcification of VSMC and valve interstitial cells (VICs) synergistically [19,20]. We found that CEC calcification is Runx2-dependent, agreeing with previous publications, demonstrating the Runx2-dependency of VSMC and VIC calcifications [10,21]. We show for the first time that hydroxyapatite accumulates in the cornea of mice with CKD. Corneal calcification was associated with elevated Runx2 expression at the site of calcification. Abnormalities in Ca and phosphate metabolism may, therefore, directly contribute to the increased susceptibility of CKD patients to corneal calcification through an active mechanism that involves Runx2-dependent calcification of CEC.

In this work, we studied the CKD-associated calcification in DBA/2J mice which is a genetically predisposed mouse strain that shows spontaneous age-dependent cardiac tissue calcification [22]. We used a diet containing adenine to induce CKD in DBA/2J mice, and high phosphate to trigger soft tissue calcification. Previously this diet was used to trigger CKD in C57BL/6 mice, in which model medial arterial and heart valve calcification and renal osteodystrophy were presented [16,17,23,24]. Concomitant with medial calcification upregulated expressions of Runx2, alkaline phosphatase, and osteopontin were shown in the aorta of CKD mice, suggesting that medial arterial calcification was driven by osteoblastic trans-differentiation of vascular smooth muscle cells. In our work, in DBA/2J mice, we found that the adenine + high phosphate diet-induced kidney dysfunction caused an elevation in urea, creatinine, and plasma phosphate levels (Fig. 1) similar to that of C57BL/6 mice. We investigated soft tissue calcification with a hydroxyapatite-specific fluorescent dye, OsteoSense, as in our previous study [17]. A major observation of this work is that besides aorta calcification, CKD induction in DBA/2J mice triggered corneal calcification (Fig. 2), providing a new *in vivo* tool for studying CKD-associated corneal calcification. Inside the cornea, we detected the calcified plaques in between the stromal and the corneal epithelial layers. Several histopathological studies reported

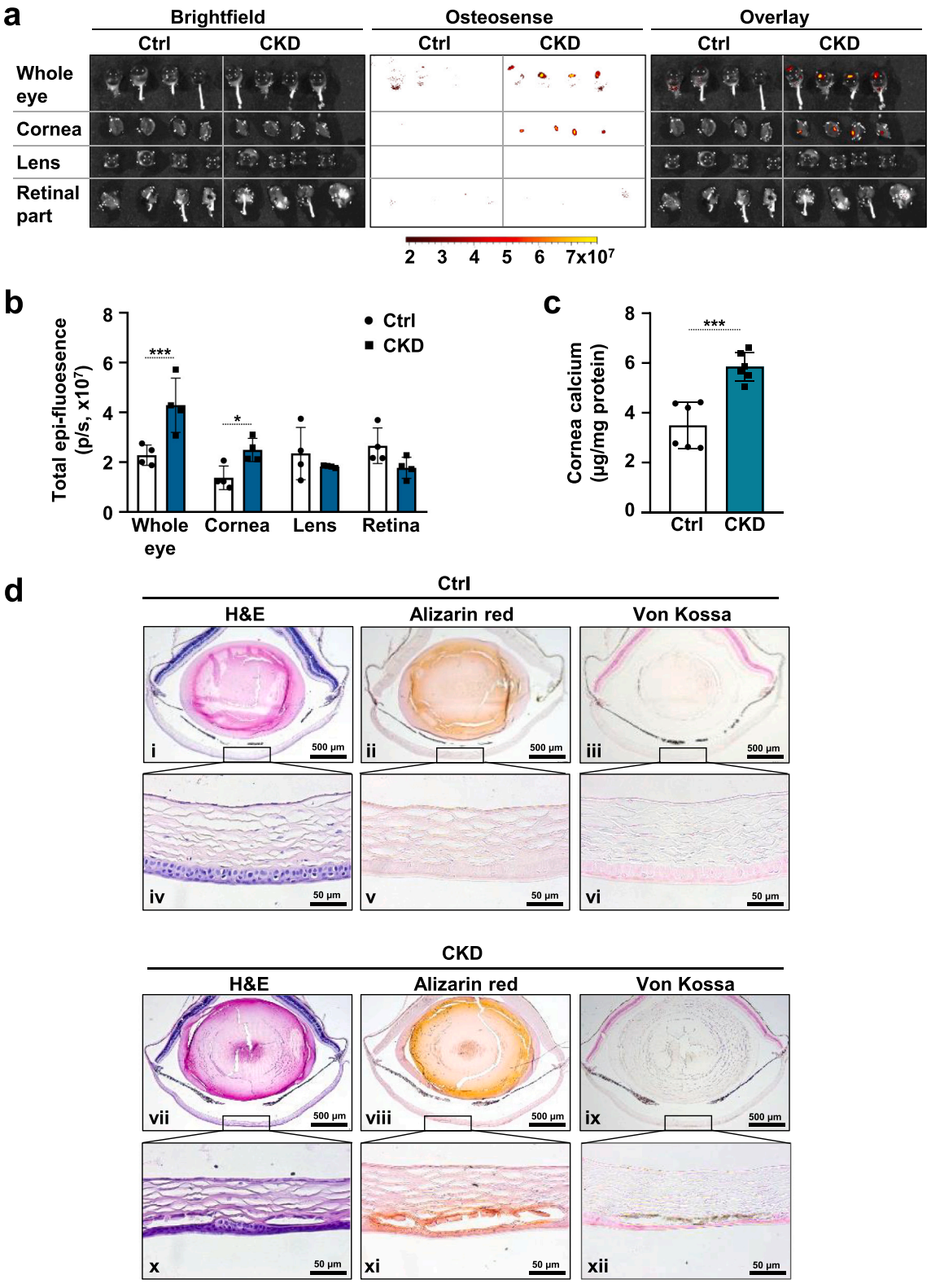

Fig. 2. Detailed analysis of eye calcification in mice with CKD.
(a) Bright-field and macroscopic fluorescence reflectance imaging of eye calcification and (b) quantification in Ctrl and CKD mice (n = 6/group). (c) Ca content of corneas derived from Ctrl and CKD mice (n = 6/group). (d) Histological analysis of eyes obtained from Ctrl and CKD mice. Representative H&E, Alizarin red, and von Kossa-stained eye sections. Scale bars: i–iii and vii-ix: 500 µm; iv-vi and x-xii: 50 µm. Data are expressed as mean ± SD. Ordinary one-way ANOVA followed by Tukey's multiple comparisons test was used to calculate p values. * $p < 0.05$, *** $p < 0.005$, **** $p < 0.001$

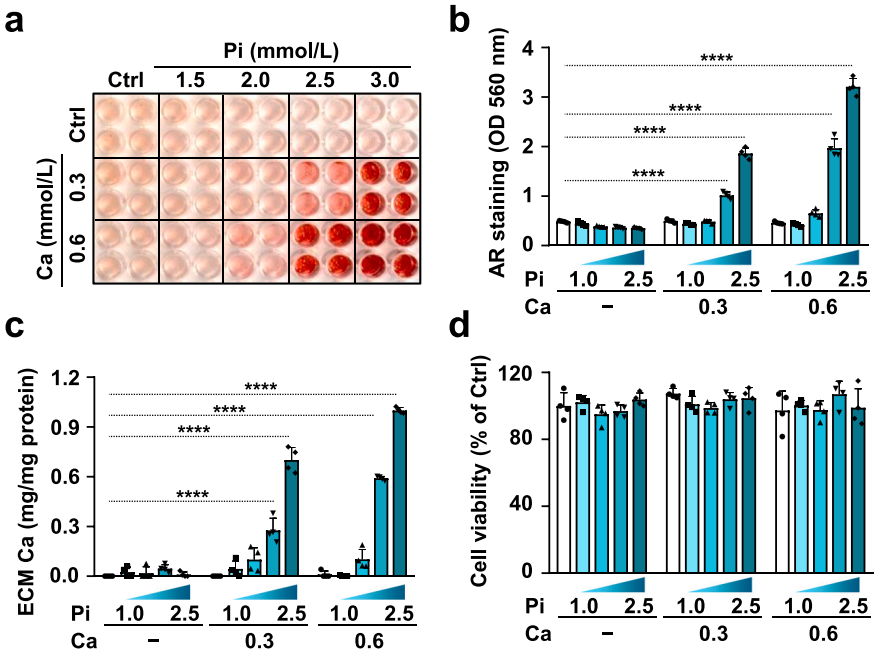

Fig. 3. Phosphate and Ca synergistically induce extracellular matrix mineralization in corneal epithelial cells (CECs).
(a–b) Confluent CECs were cultured in control (Ctrl) or osteogenic medium (OM) containing excess phosphate (Pi, 1.5–3.0 mmol/L) and excess Ca (0.3 or 0.6 mmol/L). Ca deposition in the extracellular matrix (ECM) (day 10) was evaluated by alizarin red (AR) staining. (a) Representative image and (b) quantification are depicted from 3 independent experiments. (c) Ca content of the HCl-solubilized ECM. (d) Cell viability was measured by MTT assay. Data are expressed as mean ± SD. Ordinary one-way ANOVA followed by Tukey's multiple comparison test was used to calculate *p* values. ****$p < 0.001$

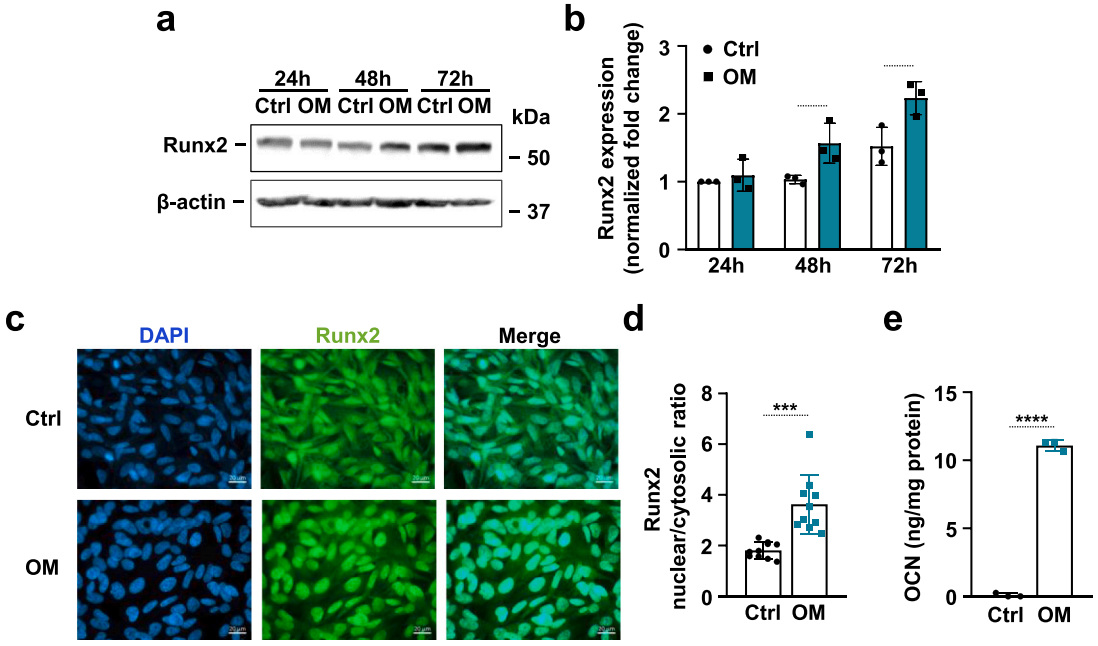

Fig. 4. Osteogenic stimuli induce calcification of CECs in a Runx2-dependent manner.
Confluent CECs were cultured in Ctrl or osteogenic conditions (OM, 2.5 mmol/L excess Pi, 0.6 mmol/L excess Ca over Ctrl). (a–b) Runx2 protein expressions detected by Western Blot from whole cell lysate (24, 48, 72 h). Membranes were re-probed for β-actin. (a) Representative Western blots and (b) densitometry analysis from 3 independent experiments. (c) CECs were cultured in Ctrl or OM conditions for 24 h. DAPI (4′,6-diamidino-2-phenylindole, blue), and Runx2 staining (green) are shown. Scale bar: 50 μm. (d) Percentage of cells with nuclear Runx2 expression. (e) Osteocalcin (OCN) expression in EDTA-solubilized ECM. Data are expressed as mean ± SD. Ordinary one-way ANOVA followed by Tukey's multiply comparison test was used to calculate *p* values: * $p < 0.05$, *** $p < 0.005$, **** $p < 0.001$.

similar calcification patterns in the cornea in human patients [25,26], mice [27,28], and rats [29].

Vascular and valve calcifications are driven by a phenotypic switch of VSMCs and VICs, respectively, whereby they gain osteoblast-like properties [30]. In this work, we asked whether corneal calcification can be an active, cell-mediated process that is similar to vascular and valve calcification, or it is just a spontaneous precipitation of hydroxyapatite. To this end, we set up an *in vitro* model in which we exposed

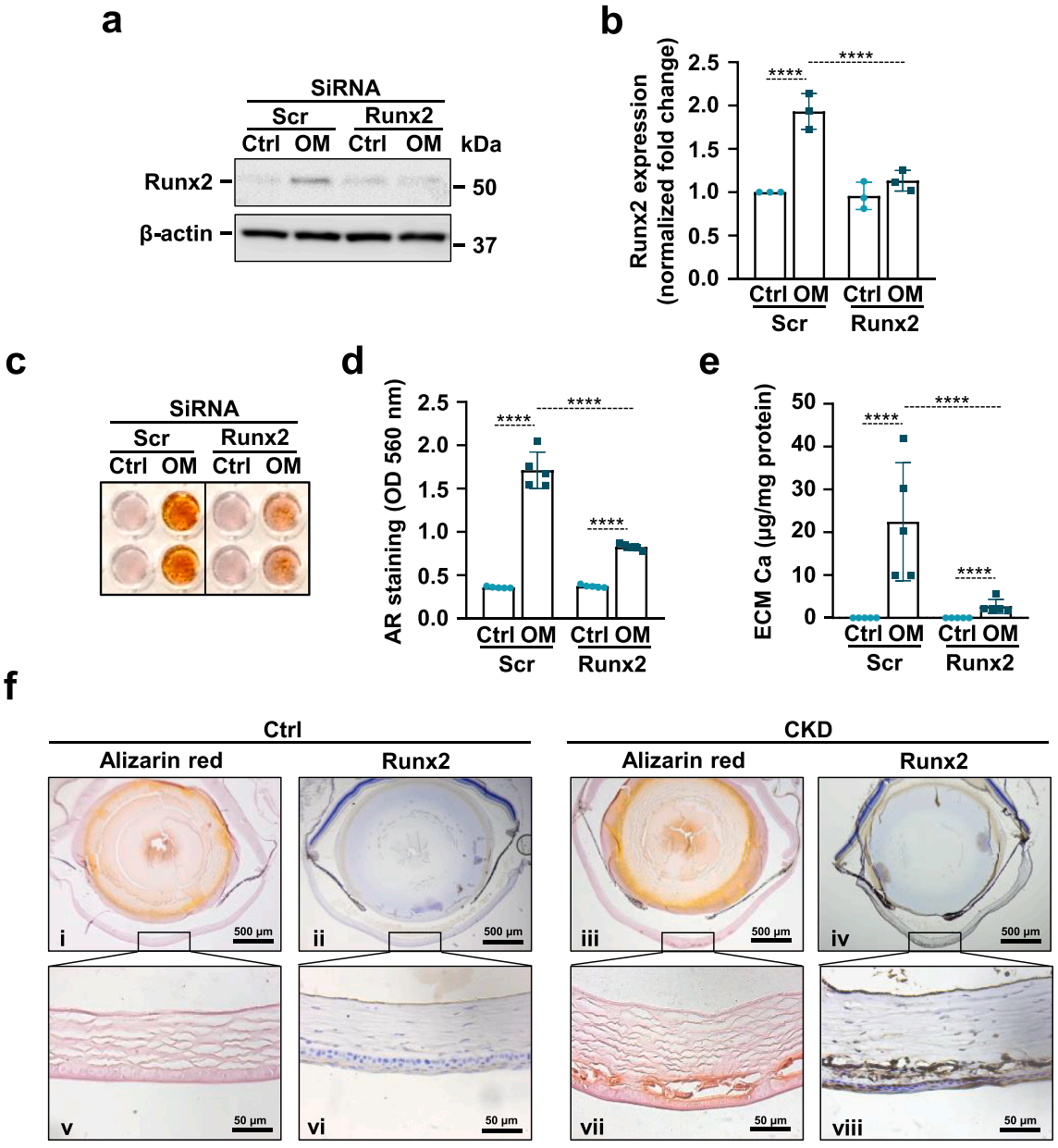

Fig. 5. Runx2 is critical for the osteogenic trans-differentiation and calcification of CECs.
Confluent CECs were cultured in Ctrl or osteogenic conditions (OM, 2.5 mmol/L excess Pi, 0.6 mmol/L excess Ca over Ctrl) in the presence of Runx2 or scrambled siRNA. (a–b) Runx2 expression detected by Western Blot from whole cell lysate (24 h). Membranes were re-probed for β-actin. (a) Representative Western blots and (b) densitometry analysis from 3 independent experiments. (c–d) Representative AR staining (day 3) and quantification (e) Ca content of the HCl-solubilized ECM. (f) Immunohistochemistry staining of eyes obtained from Ctrl and CKD mice. Representative images of Alizarin red staining and Runx2 immunoreactivity in the corneal epithelium. Scale bars: i–iv: 500 µm; v–viii: 50 µm. Data are expressed as mean ± SD. One-way ANOVA followed by Tukey's multiply comparison test was used to calculate p values. $^{*}p < 0.05$, $^{***}p < 0.005$, $^{****}p < 0.001$.

CECs to an osteogenic medium with elevated phosphate and Ca content. We chose this osteogenic stimulus since patients with late stages of CKD have elevated circulating Ca and phosphate, and because previous studies showed that increased Ca and/or phosphate induces calcification of VSMCs and VICs independently and synergistically in a modifiable cell-mediated process [19,20,24,31]. Therefore, elevated phosphate and Ca levels are considered to be the most physiologically relevant drivers of cardiovascular calcification in the late stages of CKD [32,33]. Similarly, to the above-mentioned previous observations on VSMCs and VICs [19,20,24,31], here we showed that elevation of phosphate and Ca levels induce calcification of CECs in a synergistic manner (Fig. 3).

Runx2, a member of the family of RUNX transcription factors, exhibits a wide range of biological functions. It is a fate-determining transcription factor in the differentiation of osteoblasts and chondrocytes [34]. The RUNX family of transcription factors heterodimerizes with the core binding factor β which largely enhances their DNA-binding ability [35]. Runx2 is involved in the pathomechanism of diverse diseases including cancers and cardiovascular diseases *via* affecting cell proliferation, apoptosis, autophagy, metastasis, and osteo-/chondrogenic differentiation. Importantly, Runx2 regulates the phenotype switch of VSMCs towards osteo-/chondrogenesis and thereby influences vascular calcification [10,11,21].

Runx2 is expressed and involved in diverse processes in different types of epithelial cells. For example, in mammary epithelial cells, Runx2 is implicated in the normal regulation of gene expression and tissue regeneration [36,37]. A pile of evidence shows the role of Runx2

in regulating epithelial-mesenchymal transition in normal and cancerous tissues [38–40]. Runx2 is expressed in CECs and its expression has been linked to central corneal thickness and corneal biomechanics [12–15].

Here we confirmed that CECs express Runx2 and reported that CEC calcification is associated with elevated expression and nuclear translocation of Runx2 (Fig. 4). Runx2 exerts its effects as a transcription factor within the nucleus and some studies suggested that post-translational modifications *i.e.* phosphorylation, acetylation, and ubiquitination may be required for Runx2 activation [41]. Whether these post-translational modifications played a role in osteogenic medium-induced nuclear translocation of Runx2 must be investigated further.

Silencing of Runx2 attenuated the calcification of CECs, suggesting a regulatory role of Runx2 in the calcification process (Fig. 4). Runx2 expression is increased in calcified vessels and heart valves. We found elevated expression of Runx2 in the calcified cornea of CKD mice (Fig. 5), suggesting that a common Runx2-mediated mechanism is involved in cardiovascular and corneal calcification.

CKD is a progressive condition that affects >10 % of the general population worldwide, corresponding to over 800 million individuals [42]. The frequency of eye manifestations and vision impairment is high among CKD patients, however, currently, there is no recommendation for screening for ocular diseases in this population [43]. Considering the increasing prevalence of CKD due to population aging the burden of eye diseases and vision impairment in CKD patients is likely to rise [43]. Treatment options for CKD-associated ocular diseases are limited due to a lack of complete understanding of the etiology of these diseases which warrants the development of proper disease models and further research in this field. In this study, we established an *in vivo* mice model of CKD-associated corneal calcification and suggested that a Runx2-regulated phenotype transition of CECs towards osteoblast-like cells is implicated in corneal calcification. This novel approach might initiate further research to identify new therapeutic targets to prevent or treat CKD-associated corneal calcification.

Funding statement

This work was funded by the Hungarian National Research, Development and Innovation Office (NKFIH) [K146669 to VJ and FK135327 to BN]; the Hungarian Academy of Sciences [MTA-DE Lendület Vascular Pathophysiology Research Group, grant number 96050 to VJ]. EB was supported by the János Bolyai Research Scholarship of the Hungarian Academy of Sciences (BO/00443/21) and by ÚNKP-23-5-DE-499.

Ethics approval

Animal experiments presented in this study were performed in line with the principles of the Declaration of Helsinki and the ARRIVE guidelines. Approval was granted by the Ethics Committee of the University under the registration number 10/2021/DEMÁB.

CRediT authorship contribution statement

Haneen Ababneh: Writing – review & editing, Writing – original draft, Investigation, Formal analysis, Data curation, Conceptualization. **Andrea Tóth:** Writing – review & editing, Investigation, Data curation. **Gréta Lente:** Writing – review & editing, Investigation, Data curation. **Enikő Balogh:** Writing – review & editing, Investigation, Data curation. **Dávid Máté Csiki:** Writing – review & editing, Investigation, Data curation. **Béla Nagy:** Writing – review & editing, Investigation, Funding acquisition, Data curation. **Árpád Szöőr:** Writing – review & editing, Investigation, Data curation. **Viktória Jeney:** Writing – review & editing, Writing – original draft, Supervision, Funding acquisition, Formal analysis, Conceptualization.

Declaration of competing interest

The authors have no relevant financial or non-financial interests to disclose.

Data availability

Data will be made available on request.

References

[1] N.R. Hill, S.T. Fatoba, J.L. Oke, J.A. Hirst, C.A. O'Callaghan, D.S. Lasserson, F.D. R. Hobbs, Global prevalence of chronic kidney disease — a systematic review and meta-analysis, PloS One 11 (2016), https://doi.org/10.1371/JOURNAL.PONE.0158765.

[2] K.A. Hruska, S. Mathew, R. Lund, P. Qiu, R. Pratt, Hyperphosphatemia of chronic kidney disease, Kidney Int. 74 (2008) 148, https://doi.org/10.1038/KI.2008.130.

[3] R. Porter, A.L. Crombie, Corneal and conjunctival calcification in chronic renal failure, Br. J. Ophthalmol. 57 (1973) 339–343, https://doi.org/10.1136/BJO.57.5.339.

[4] N. Klaassen-Broekema, O.P. Van Bijsterveld, Limbal and corneal calcification in patients with chronic renal failure, Br. J. Ophthalmol. 77 (1993) 569–571, https://doi.org/10.1136/BJO.77.9.569.

[5] N. Seyahi, M.R. Altiparmak, A. Kahveci, H. Yetik, K. Kanberoglu, K. Serdengecti, R. Ataman, E. Erek, Association of conjunctival and corneal calcification with vascular calcification in dialysis patients, Am. J. Kidney Dis. 45 (2005) 550–556, https://doi.org/10.1053/j.ajkd.2004.11.002.

[6] M.B.C.N. Pessoa, R.M. Santo, A.A. de Deus, E.J. Duque, S.F. Crispilho, V. Jorgetti, M.A. Dalboni, C.E. Rochitte, R.M.A. Moyses, R.M. Elias, Corneal and coronary calcification in maintenance hemodialysis: the face is no index to the heart, JBMR Plus 7 (2023) e10823, https://doi.org/10.1002/jbm4.10823.

[7] L. Spadea, M.I. Giannico, A. Iannaccone, S. Pistella, Excimer laser-assisted phototherapeutic keratectomies combined to EDTA chelation for the treatment of calcific band keratopathy, Eur. J. Ophthalmol. 32 (2022) NP42–NP46, https://doi.org/10.1177/1120672120969033.

[8] C.H. Hsiao, A. Chao, S.Y. Chu, K.K. Lin, L. Yeung, D.T. Lin-Tan, J.L. Lin, Association of severity of conjunctival and corneal calcification with all-cause 1-year mortality in maintenance haemodialysis patients, Nephrol. Dial. Transplant. 26 (2011) 1016–1023, https://doi.org/10.1093/NDT/GFQ485.

[9] A.P. Sage, Y. Tintut, L.L. Demer, Regulatory mechanisms in vascular calcification, Nat. Rev. Cardiol. 7 (2010) 528–536, https://doi.org/10.1038/NRCARDIO.2010.115.

[10] M.Y. Speer, X. Li, P.G. Hiremath, C.M. Giachelli, Runx2/Cbfa1, but not loss of myocardin, is required for smooth muscle cell lineage reprogramming toward osteochondrogenesis, J. Cell. Biochem. 110 (2010) 935–947, https://doi.org/10.1002/JCB.22607.

[11] Y. Sun, C.H. Byon, K. Yuan, J. Chen, X. Mao, J.M. Heath, A. Javed, K. Zhang, P. G. Anderson, Y. Chen, Smooth muscle cell-specific runx2 deficiency inhibits vascular calcification, Circ. Res. 111 (2012) 543–552, https://doi.org/10.1161/CIRCRESAHA.112.267237.

[12] M.T. Ortiz-Melo, M.J. Garcia-Murillo, V.M. Salazar-Rojas, J.E. Campos, F. Castro-Muñozledo, Transcriptional profiles along cell programming into corneal epithelial differentiation, Exp. Eye Res. 202 (2021) 108302, https://doi.org/10.1016/j.exer.2020.108302.

[13] A.I. Iglesias, A. Mishra, V. Vitart, Y. Bykhovskaya, R. Höhn, H. Springelkamp, G. Cuellar-Partida, P. Gharahkhani, J.N.C. Bailey, C.E. Willoughby, X. Li, S. Yazar, A. Nag, A.P. Khawaja, O. Polašek, D. Siscovick, P. Mitchell, Y.C. Tham, J.L. Haines, L.S. Kearns, C. Hayward, Y. Shi, E.M. van Leeuwen, K.D. Taylor, P. Bonnemaijer, J. I. Rotter, N.G. Martin, T. Zeller, R.A. Mills, E. Souzeau, S.E. Staffieri, J.B. Jonas, I. Schmidtmann, T. Boutin, J.H. Kang, S.E.M. Lucas, T.Y. Wong, M.E. Beutel, J. F. Wilson, A.G. Uitterlinden, E.N. Vithana, P.J. Foster, P.G. Hysi, A.W. Hewitt, C. C. Khor, L.R. Pasquale, G.W. Montgomery, C.C.W. Klaver, T. Aung, N. Pfeiffer, D. A. Mackey, C.J. Hammond, C.-Y. Cheng, J.E. Craig, Y.S. Rabinowitz, J.L. Wiggs, K. P. Burdon, C.M. van Duijn, S. MacGregor, Cross-ancestry genome-wide association analysis of corneal thickness strengthens link between complex and Mendelian eye diseases, Nat. Commun. 9 (2018) 1864, https://doi.org/10.1038/s41467-018-03646-6.

[14] Z. Yang, J. Yang, D. Liu, W. Yu, Mendelian randomization analysis identified genes pleiotropically associated with central corneal thickness, BMC Genomics 22 (2021) 517, https://doi.org/10.1186/s12864-021-07860-3.

[15] X. Sun, X. Gao, B.-K. Mu, Y. Wang, Understanding the role of corneal biomechanics-associated genetic variants by bioinformatic analyses, Int. Ophthalmol. 42 (2022) 981–988, https://doi.org/10.1007/s10792-021-02081-9.

[16] T. Tani, H. Orimo, A. Shimizu, S. Tsuruoka, Development of a novel chronic kidney disease mouse model to evaluate the progression of hyperphosphatemia and associated mineral bone disease, Sci. Rep. 7 (2017), https://doi.org/10.1038/S41598-017-02351-6.

[17] A. Tóth, D.M. Csiki, B. Nagy, E. Balogh, G. Lente, H. Ababneh, Á. Szöőr, V. Jeney, Daprodustat accelerates high phosphate-induced calcification through the activation of HIF-1 signaling, Front. Pharmacol. 13 (2022), https://doi.org/10.3389/FPHAR.2022.798053.

[18] T. Tokuyama, T. Ikeda, K. Sato, O. Mimura, A. Morita, T. Tabata, Conjunctival and corneal calcification and bone metabolism in hemodialysis patients, Am. J. Kidney Dis. 39 (2002) 291–296, https://doi.org/10.1053/ajkd.2002.30548.
[19] J.L. Reynolds, A.J. Joannides, J.N. Skepper, R. Mcnair, L.J. Schurgers, D. Proudfoot, W. Jahnen-Dechent, P.L. Weissberg, C.M. Shanahan, Human vascular smooth muscle cells undergo vesicle-mediated calcification in response to changes in extracellular calcium and phosphate concentrations: a potential mechanism for accelerated vascular calcification in ESRD, J. Am. Soc. Nephrol. 15 (2004) 2857–2867, https://doi.org/10.1097/01.ASN.0000141960.01035.28.
[20] L. Cui, N.A. Rashdan, D. Zhu, E.M. Milne, P. Ajuh, G. Milne, M.H. Helfrich, K. Lim, S. Prasad, D.A. Lerman, A.T. Vesey, M.R. Dweck, W.S. Jenkins, D.E. Newby, C. Farquharson, V.E. Macrae, End stage renal disease-induced hypercalcemia may promote aortic valve calcification via Annexin VI enrichment of valve interstitial cell derived-matrix vesicles, J. Cell. Physiol. 232 (2017) 2985–2995, https://doi.org/10.1002/jcp.25935.
[21] S. Dharmarajan, M.Y. Speer, K. Pierce, J. Lally, E.M. Leaf, M.-E. Lin, M. Scatena, C. M. Giachelli, Role of Runx2 in calcific aortic valve disease in mouse models, Front. Cardiovasc. Med. 8 (2021), https://doi.org/10.3389/FCVM.2021.687210.
[22] R.W. Rings, J.E. Wagner, Incidence of cardiac and other soft tissue mineralized lesions in DNA-2 mice, Lab. Anim. Sci. 22 (1972) 344–352.
[23] X. Yang, Y. Liu, X. Zhu, P. Chen, X. Xie, T. Xu, X. Zhang, Y. Zhao, Vascular, valvular and kidney calcification manifested in mouse models of adenine-induced chronic kidney disease, Ren. Fail. 45 (2023) 2228920, https://doi.org/10.1080/0886022X.2023.2228920.
[24] D.M. Csiki, H. Ababneh, A. Tóth, G. Lente, Á. Szöőr, A. Tóth, C. Fillér, T. Juhász, B. Nagy, E. Balogh, V. Jeney, Hypoxia-inducible factor activation promotes osteogenic transition of valve interstitial cells and accelerates aortic valve calcification in a mice model of chronic kidney disease, Front. Cardiovasc. Med. 10 (2023), https://doi.org/10.3389/FCVM.2023.1168339/FULL.
[25] G.R. O'Connor, Calcific band keratopathy, Trans. Am. Ophthalmol. Soc. 70 (1972) 58–81.
[26] R. Arora, D. Shroff, S. Kapoor, S. Nigam, R. Narula, D. Chauhan, P. Jain, Familial calcific band-shaped keratopathy: report of two new cases with early recurrence, Indian J. Ophthalmol. 55 (2007) 55–57, https://doi.org/10.4103/0301-4738.29496.
[27] D. Koehn, K.J. Meyer, N.A. Syed, M.G. Anderson, Ketamine/xylazine-induced corneal damage in mice, PloS One 10 (2015) e0132804, https://doi.org/10.1371/journal.pone.0132804.
[28] R. Mittl, M.A. Galin, W. Opperman, R.A. Camerini-Davalos, D. Spiro, Corneal calcification in spontaneously daibetic mice, Invest. Ophthalmol. 9 (1970) 137–145.
[29] S. Hashimoto, T. Doi, Y. Wako, J. Sato, S. Wada, M. Tsuchitani, Corneal mineralization in wistar hannover rats, J. Toxicol. Pathol. 26 (2013) 275–281, https://doi.org/10.1293/tox.26.275.
[30] L. Hortells, S. Sur, C. St Hilaire, Cell phenotype transitions in cardiovascular calcification, Front. Cardiovasc. Med. 5 (2018) 27, https://doi.org/10.3389/fcvm.2018.00027.
[31] E. Balogh, A. Tóth, G. Méhes, G. Trencsényi, G. Paragh, V. Jeney, Hypoxia triggers osteochondrogenic differentiation of vascular smooth muscle cells in an HIF-1 (hypoxia-inducible factor 1)-dependent and reactive oxygen species-dependent manner, Arterioscler. Thromb. Vasc. Biol. 39 (2019) 1088–1099, https://doi.org/10.1161/ATVBAHA.119.312509.
[32] S. Yamada, C.M. Giachelli, Vascular calcification in CKD-MBD: roles for phosphate, FGF23, and Klotho, Bone 100 (2017) 87–93, https://doi.org/10.1016/j.bone.2016.11.012.
[33] C.M. Giachelli, The emerging role of phosphate in vascular calcification, Kidney Int. (2009), https://doi.org/10.1038/ki.2008.644.
[34] T. Komori, Regulation of osteoblast differentiation by Runx2, Adv. Exp. Med. Biol. 658 (2010) 43–49, https://doi.org/10.1007/978-1-4419-1050-9_5.
[35] C.A. Yoshida, T. Furuichi, T. Fujita, R. Fukuyama, N. Kanatani, S. Kobayashi, M. Satake, K. Takada, T. Komori, Core-binding factor beta interacts with Runx2 and is required for skeletal development, Nat. Genet. 32 (2002) 633–638, https://doi.org/10.1038/NG1015.
[36] C.K. Inman, P. Shore, The osteoblast transcription factor Runx2 is expressed in mammary epithelial cells and mediates osteopontin expression, J. Biol. Chem. 278 (2003) 48684–48689, https://doi.org/10.1074/jbc.M308001200.
[37] N. Ferrari, A.I. Riggio, S. Mason, L. McDonald, A. King, T. Higgins, I. Rosewell, J. C. Neil, M.J. Smalley, O.J. Sansom, J. Morris, E.R. Cameron, K. Blyth, Runx2 contributes to the regenerative potential of the mammary epithelium, Sci. Rep. 5 (2015) 15658, https://doi.org/10.1038/srep15658.
[38] A.L.P. Tavares, J.A. Brown, E.C. Ulrich, K. Dvorak, R.B. Runyan, Runx2-I is an early regulator of epithelial-mesenchymal cell transition in the chick embryo, Dev. Dyn. 247 (2018) 542–554, https://doi.org/10.1002/dvdy.24539.
[39] A.M. Herreño, A.C. Ramírez, V.P. Chaparro, M.J. Fernandez, A. Cañas, C. F. Morantes, O.M. Moreno, R.E. Brugés, J.A. Mejía, F.J. Bustos, M. Montecino, A. P. Rojas, Role of RUNX2 transcription factor in epithelial mesenchymal transition in non-small cell lung cancer lung cancer: epigenetic control of the RUNX2 P1 promoter, Tumour Biol. J. Int. Soc. Oncodev. Biol. Med. 41 (2019), https://doi.org/10.1177/1010428319851014, 1010428319851014.
[40] D.-F. Niu, T. Kondo, T. Nakazawa, N. Oishi, T. Kawasaki, K. Mochizuki, T. Yamane, R. Katoh, Transcription factor Runx2 is a regulator of epithelial-mesenchymal transition and invasion in thyroid carcinomas, Lab. Invest. 92 (2012) 1181–1190, https://doi.org/10.1038/labinvest.2012.84.
[41] M. Bruderer, R.G. Richards, M. Alini, M.J. Stoddart, Role and regulation of RUNX2 in osteogenesis, Eur. Cell. Mater. 28 (2014) 269–286, https://doi.org/10.22203/ecm.v028a19.
[42] C.P. Kovesdy, Epidemiology of chronic kidney disease: an update 2022, Kidney Int. Suppl. 12 (2022) 7–11, https://doi.org/10.1016/j.kisu.2021.11.003.
[43] S. Nusinovici, C. Sabanayagam, B.W. Teo, G.S.W. Tan, T.Y. Wong, Vision impairment in CKD patients: epidemiology, mechanisms, differential diagnoses, and prevention, Am. J. Kidney Dis. 73 (2019) 846–857, https://doi.org/10.1053/j.ajkd.2018.12.047.